AIAA SciTech Forum
6-10 January 2020, Orlando, FL
AIAA Scitech 2020 Forum

10.2514/6.2020-2042

Single-component molecular tagging velocimetry of the boundary layer on a NACA-0012 airfoil plunging across uniform-shear flow

Mitchell B. Albrecht,* Ahmed M. Naguib,† and Manoochehr M. Koochesfahani‡
Michigan State University, East Lansing, Michigan, 48824

Molecular tagging velocimetry is used to measure the streamwise velocity component of the flow over the suction side of a NACA-0012 airfoil plunging across a uniform-shear approach flow in a water tunnel. The flow over the plunging airfoil is compared to that of the stationary airfoil at the same effective angles of attack, under the same flow conditions. The boundary layer on the airfoil is investigated in the context of previous lift coefficient measurements under the same flow conditions. The flow over the plunging airfoil at small effective angles of attack is found to be similar to its stationary counterpart, consistent with their similar lift coefficients. However, at positive angles of attack, near stall, the flow over the plunging airfoil exhibits greatly different separation and reattachment characteristics compared to the stationary airfoil. Specifically, a separation bubble forms on the plunging airfoil at a lower effective angle of attack, with the corresponding separation and reattachment locations closer to the leading edge. The flow phenomena in the positive, near-stall angle of attack range correspond to the higher lift coefficient on the plunging airfoil versus the stationary airfoil.

I. Nomenclature

AR	=	aspect ratio
b	=	airfoil span
C_L	=	lift coefficient
c	=	airfoil chord
du_∞/dY	=	shear rate
f	=	image acquisition frequency
K	=	non-dimensional shear rate of flow; $(du_\infty/dY) \times (c/u_0)$
Re_c	=	chord Reynolds number; $u_0 c/\nu$
t	=	time
u	=	streamwise velocity
u'	=	streamwise velocity in the Galilean reference frame
u_∞	=	freestream velocity
u_0	=	approach freestream velocity at y-coordinate of the airfoil ¼-chord
u_1	=	uniform high-speed flow region velocity
u_2	=	uniform low-speed flow region velocity
u_{eff}	=	effective freestream velocity relative to airfoil ¼-chord; $\sqrt{u_0^2 + V_a^2} = u_0\sqrt{1 + V_r^2}$
u'_{rms}	=	fluctuating streamwise velocity RMS in the Galilean reference frame
u_{rms}	=	fluctuating streamwise velocity RMS
$\dot{u}_0^+$	=	flow unsteadiness parameter in the Galilean reference frame; $K \times V_r$
V_a	=	airfoil plunge velocity
V_r	=	velocity ratio; $\lvert V_a \rvert / u_0$
v	=	cross-stream velocity
x	=	streamwise coordinate relative to airfoil ¼-chord
x'	=	streamwise coordinate relative to airfoil ¼-chord in the Galilean reference frame
x^*	=	chord-wise coordinate relative to airfoil leading edge
Y	=	cross-stream coordinate relative to tunnel centerline
y	=	cross-stream coordinate at the airfoil ¼-chord in the laboratory reference frame

* Graduate Student, Mechanical Engineering, 1449 Engineering Research Ct A108, East Lansing, MI 48824, AIAA Member.
† Professor, Mechanical Engineering, 1449 Engineering Research Ct C128, East Lansing, MI 48824, AIAA Associate Fellow.
‡ Professor, Mechanical Engineering, 1449 Engineering Research Ct A131, East Lansing, MI 48824, AIAA Associate Fellow.

y' = cross-stream coordinate at the airfoil ¼-chord in the Galilean reference frame
y^* = chord-normal coordinate
α = geometric angle of attack
α_{eff} = effective angle of attack; $\alpha + \alpha_i$
α_i = angle of attack induced by plunging motion; $\tan^{-1}(|V_a|/u_0) = \tan^{-1}(V_r)$
Δt = time delay
δ = shear layer width
ν = kinematic viscosity

II. Introduction

A large body of work has investigated the effects of unsteadiness on airfoils resulting from gusts, wakes, plunging, and pitching, based on uniform or periodic approach stream conditions. However, a non-uniform (shear) freestream approach condition may be more appropriate in many applications. Air currents in urban environments [1, 2], atmospheric boundary layers [3], and aircraft carrier air wakes [4, 5] are just a few examples of such applications that are experienced regularly by aerodynamic bodies over a large range of scales from micro air vehicles (MAVs) to jet aircraft. The fundamental aerodynamics of an airfoil in the presence of a viscous shear approach stream is only just being discovered. Recent work shows a negative mean C_L to occur at zero angle of attack (AoA) on a steady, symmetric airfoil in positive shear [6], opposite of inviscid theory [7]. The magnitude of this negative mean C_L increases with increasing shear rate [6]. Compared to uniform flow, the harmonically-pitching airfoil in shear exhibits significantly different wake and lift behavior [8]. Previous work on a NACA-0012 airfoil plunging unidirectionally across a steady positive-uniform-shear approach stream exhibits change in stall characteristics relative to the stationary airfoil [9, 10]. In comparison to the stationary airfoil, the plunging airfoil maximum C_L increases, and the stall angle decreases, as shown in Fig. 1, when analyzed in a Galilean transformation (GT) reference frame. The current work is an extension of the work in Refs. [9] and [10], undertaken to explore the flow behavior underlying the similarities and the differences in lift behavior between the stationary and moving airfoils. Finding a connection between these two cases has the practical ramification of alleviating the need to perform research on a moving model, in favor of a stationary model. The C_L measurements in Fig. 1 show that, in a GT frame of reference, the moving airfoil exhibits the same C_L characteristics as the stationary airfoil for small and negative AoAs. This implies that the flow is quasi-steady (QS) for this AoA range, hence the load acting on the moving airfoil can be deduced from the stationary airfoil. As described below, the fundamental nature of the unsteadiness in this case is the changing approach stream velocity as the airfoil traverses across the shear zone. Such unsteadiness is not present for an airfoil traversing steadily across *uniform* approach flow, where the stationary airfoil aerodynamics can be completely determined from those of the stationary airfoil.

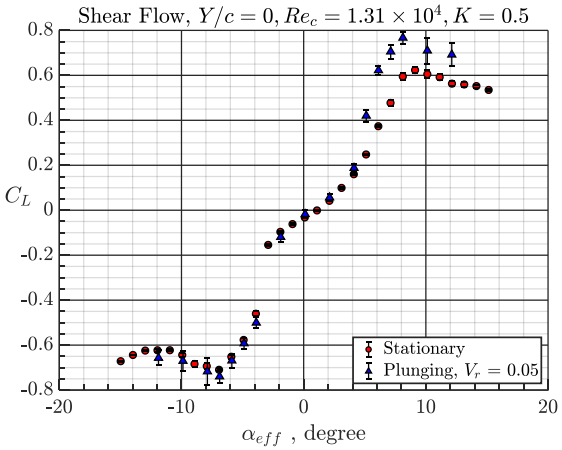

Fig. 1 Comparison of the mean C_L on the stationary and the plunging airfoil in uniform-shear flow along the tunnel centerline [9].

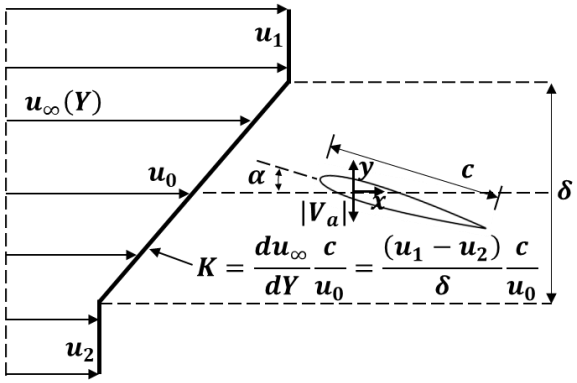

Fig. 2 Schematic of the translating airfoil in positive uniform-shear flow.

This work addresses the above objective by conducting boundary-layer-resolved measurements of the streamwise component of the velocity field on the suction surface of a NACA-0012 airfoil plunging across a positive-uniform-shear flow. That is, as sketched in Fig. 2, the freestream velocity changes linearly with a uniform gradient du_∞/dY, such that the airfoil traveling at velocity V_a in the negative-Y direction with a geometric AoA α experiences a decreasing approach stream velocity. A velocity scale u_0 is used to characterize the local approach stream velocity at

the cross-stream coordinate of the airfoil ¼-chord point (see Fig. 2). The motion of the airfoil creates an induced AoA α_i, which, in the GT reference frame, results in an effective AoA α_{eff} and local effective approach velocity u_{eff} (see Fig. 3). The unsteadiness of the flow relative to the airfoil may be characterized by the non-dimensional rate of change of u_o:

$$\dot{u}_0^+ = \left(\frac{du_0}{dt}\right) \times \left(\frac{c}{u_0^2}\right) = \left(\frac{du_\infty}{dY} \times V_a\right) \times \left(\frac{c}{u_0^2}\right) = K \times V_r \tag{1}$$

where, V_r is the ratio of the airfoil velocity to u_0, and K is the non-dimensional shear rate. Based on Eq. (1), one would expect the flow to be quasi-steady in the limit $\dot{u}_0^+ \to 0$, or $V_r \to 0$ and $K \to 0$. The latter condition implies "quasi-uniformity" of the flow. For a cylinder traversing steadily across an infinitely wide uniform-shear flow, if the inviscid flow around the cylinder is quasi-steady, it is also quasi-uniform, and vice versa [11].

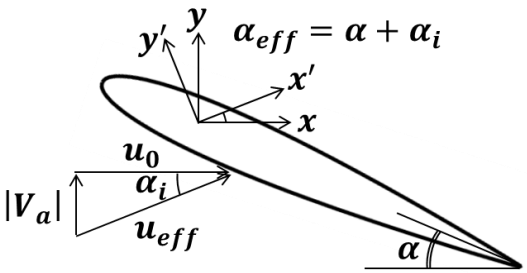

Fig. 3 Diagram defining the effective flow velocity and effective angle of attack of the plunging airfoil in the GT frame.

The flow measurements in the present work focus on capturing the boundary layer characteristics, including separation and reattachment points, for the stationary and the plunging airfoil at the chord Reynolds number $Re_c = 1.3 \times 10^4$. Measurements are conducted in a water tunnel to take advantage of an existing single-component molecular tagging velocimetry (1c-MTV) system. This method allows for high-spatial-resolution measurements near the airfoil surface, enabling resolution of the boundary layer. The work in Ref. [10] demonstrated the same qualitative lift-coefficient behavior as shown in Fig. 1 but at the higher Reynolds number $Re_c = 7.5 \times 10^4$. This suggests that the nature of the underlying flow physics at the Reynolds number of the present investigation are similar to those at Reynolds numbers that are at least five-fold higher.

III. Experimental Setup and Methods

A. Water Tunnel

Experiments are performed in the 10,000 L closed-return, free-surface water tunnel (Engineering Laboratory Design, ELD) at the Turbulent Mixing and Unsteady Aerodynamics Laboratory at Michigan State University. The tunnel has a 61 cm × 61 cm × 244 cm acrylic test section with two quartz windows on one side to allow UV laser light to enter the test section (see Fig. 4). The NACA-0012 airfoil model (c = 12 cm, b = 61 cm, AR = 5.1) is suspended in the test section by a three-degree-of-freedom servo motion system capable of pitch, plunge, and surge motions. The present work uses a Parker rotary servo motor (model number MPP1154A9D-KPSN) mounted to the carriage of a Parker linear servo motor (model number T4DB0436NPAMA4) to perform airfoil pitch and plunge motions only. The pitch motor has an angular position resolution of 0.003°, while the linear motor has a linear position resolution of 1 µm. On the upstream and downstream sides of the airfoil shaft, and spanning the test section width, are two suspended polycarbonate skimmer plates in contact with the water surface. These plates provide a well-defined boundary condition and mitigate free surface disturbances from the airfoil motion. The skimmer plates are separated

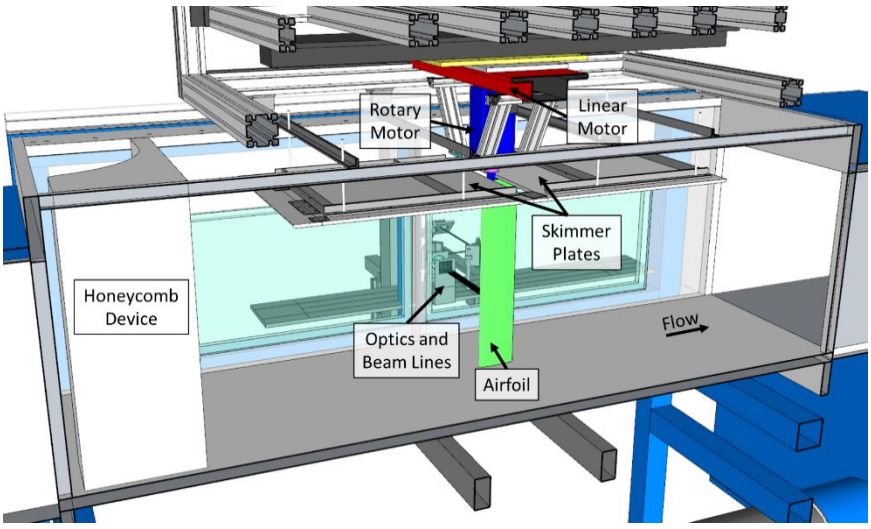

Fig. 4 Water tunnel test section highlighting the motion system, optical setup, and shear generation method.

from each other by 4.4 cm to allow the airfoil shaft to travel in the cross-stream direction. The airfoil shaft diameter is 3.8 cm, thus leaving approximately 3 mm clearance between it and each skimmer plate edge. The airfoil maintains clearance gaps between its upper tip and the skimmer plates, and its lower tip and the test section floor, of less than 0.75 mm (0.63% c) each. In the absence of shear generation, at a freestream of 10 cm/s, the flow velocity is steady and uniform across the tunnel width, with a temporal and spatial RMS of less than 2.5% and 5%, respectively.

B. Shear Generation

A shaped honeycomb is used to generate the uniform-shear freestream velocity profile in the water tunnel, based on the technique developed in Ref. [12] and refined in Ref. [13]. The honeycomb device is installed at the entrance of the test section with the high-speed side of the flow towards the positive-Y direction, as depicted in Fig. 2. The device is shaped to generate a three-segment velocity profile, consisting of a linear mean-velocity profile in between regions of high- and low-speed uniform flows, as depicted in Fig. 5 (left). The honeycomb device generates a mean-velocity profile with the non-dimensional shear layer width δ/c = 1.7, wherein the non-dimensional shear rate is K = 0.5. The corresponding temporal RMS profile, shown in Fig. 5 (right), is approximately uniform, staying within 1.5 – 2%, except at the velocity undershoot region near the low-speed edge of the shear layer, where the profile rises to about 3.2%. At the water tunnel centerline, where the measurements are referenced, the local approach freestream velocity is 10cm/s, corresponding to K = 0.5.

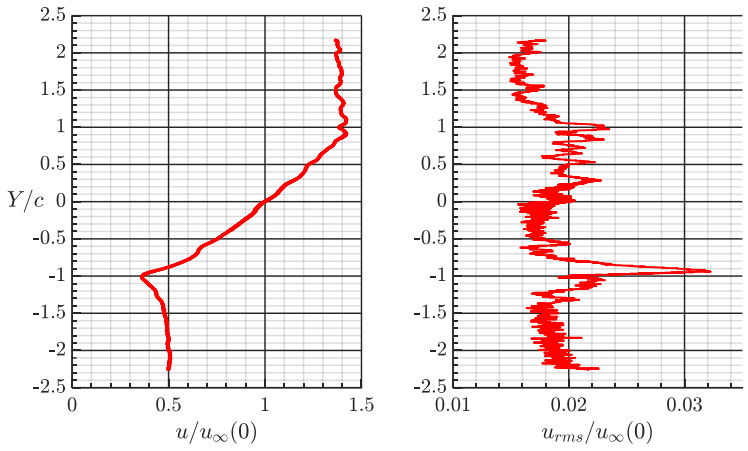

Fig. 5 Measured three-segment shear flow generated by the honeycomb shear device, with a linear mean-velocity profile in the central segment (left), and the fluctuating velocity RMS profile (right).

C. Airfoil Dynamics

For moving airfoil measurements, the airfoil starts from rest at 1.5c (18 cm) above the water tunnel centerline. To ensure that the airfoil reaches as close to steady-state as possible before entering the shear layer, the airfoil is accelerated and pitched from rest and initial α to the final V_a and α, over 0.42c (5 cm) of travel. The pitching motion profile is tailored to maintain constant α_{eff} during the initial acceleration phase of the airfoil in the uniform high-speed flow region. Figure 6 provides an example of the lift coefficient versus cross-stream position for $Re_c = 1.8 \times 10^4$ and $V_r = 0.09$, using the same force measurement methods in Ref. [9]. This demonstrates the ability of the tailored motion profile to reach steady-state before entering the equivalent position of the start of the shear layer at $Y/c = 1$. Similar measurements were performed for $V_r = 0.05$ in $Re_c = 1.3 \times 10^4$ uniform flow,

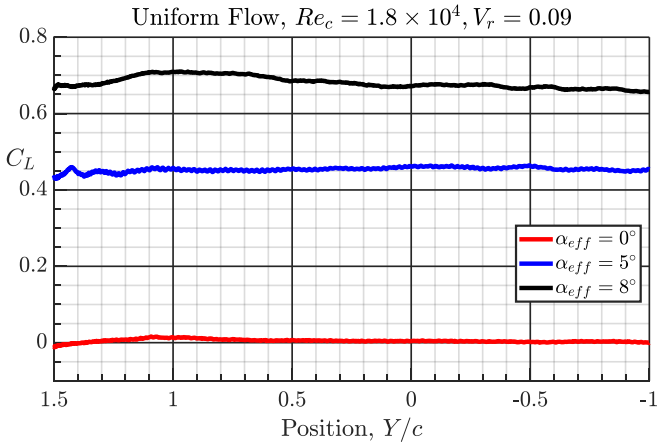

Fig. 6 Lift coefficient on the moving airfoil in uniform flow for $Re_c = 1.8 \times 10^4$, and $V_r = 0.09$, versus water tunnel cross-stream position. The Re_c is the same as that of the high-speed uniform region of the shear flow, and a high plunge speed is chosen, to demonstrate the steady-state behavior of the airfoil with the tailored motion profile to maintain α_{eff} during the initial motion phase.

which also showed steady-state behavior after the initial airfoil acceleration phase. In the shear zone, V_r (and therefore α_{eff}) increases with time due to the decrease in u_0 as the airfoil traverses across the central flow segment. Thus, the final V_a and α values reached by the airfoil before entering the shear zone are selected to produce the desired V_r and α_{eff} at the cross-stream location where measurements are performed ($Y/c = 0$) in the shear flow ($V_r = 0.05$ for this work). Once at the steady test speed and the final α, the airfoil continues across the shear layer at constant $|V_a|$ = 0.5 cm/s and α before coming to rest in the low-speed uniform region $3c$ (36 cm) from the starting position. The airfoil then returns to the starting position and α to repeat the process.

D. 1c-MTV

Molecular tagging velocimetry (MTV) is a diagnostic technique in which a flowing medium is premixed with molecules that can be turned into long-lifetime tracers upon excitation by photons of a particular wavelength [14, 15]. For this work, a COMPex*Pro* 205C XeCl 308 nm excimer laser generates pulsed beams to "tag" the regions of interest containing a phosphorescent supramolecule tracer [14]. The beam is formed into a sheet and directed into the water tunnel test section by a series of optical components, including a beam blocker that separates the sheet into many individual lines for 1c-MTV. The tagged regions along each line are interrogated at two different times, separated by Δt, within the lifetime of the tracer. Images are acquired using a PCO Pixelfly camera with a Nikon 58 mm f/1.2 lens, yielding a resolution of 1 pixel = 69 μm (approximately 0.06% c). The Lagrangian displacement in the direction normal to the tag line is measured at every pixel along the line using the spatial correlation techniques outlined in Ref. [16]. An advantage of using 1c-MTV is its high spatial resolution in measuring flow phenomena near boundaries. Figure 7 provides a sample set of 1c-MTV images over the NACA-0012 airfoil at α = 6° in shear flow at the two separate times relative to the laser pulse. The airfoil boundary layer and near-wake can be seen in the deformation of the lines in the "delayed" image relative to the "undelayed" image.

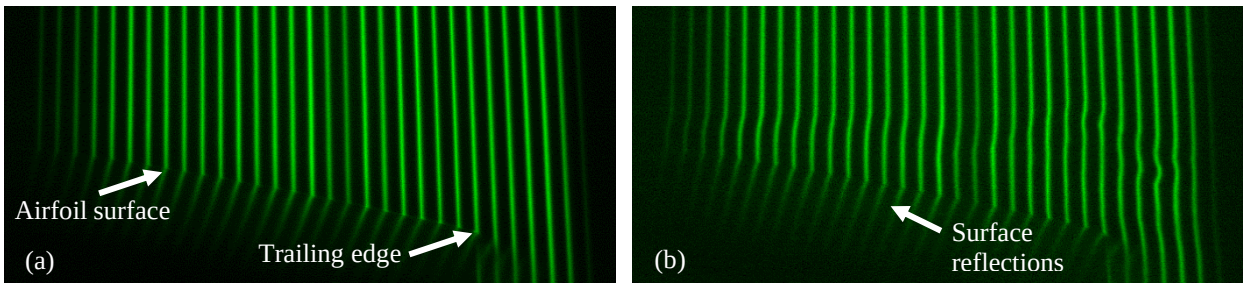

Fig. 7 Instantaneous images of the 1c-MTV beam lines for a stationary airfoil at α = 6°: (a) 3 μs after the laser pulse ("undelayed"), and (b) Δt = 5 ms later ("delayed"). Both images are 1392 pixel × 631 pixel ($0.8c \times 0.36c$), and the flow is from left to right. Tagged regions are given by the green lines produced by phosphorescence emission.

Images are acquired in two fields of view (FOV) along the airfoil chord to obtain line spacing with a chord-wise resolution of around 2.5% c or less. At the airfoil speed used in the current study, each plunge cycle takes a long time to complete. Thus, only 50 strokes are recorded for the plunging airfoil cases, except for the case of $\alpha_{eff} = 8°$ which uses 100 strokes to try to account for the higher flow unsteadiness encountered at this AoA. A single delayed image is recorded in each stroke when the airfoil is at the center of the tunnel ($Y/c = 0$), triggered by the linear positioner encoder, which has a resolution of 1 μm (<0.001% c). In contrast, for the stationary airfoil measurements, 1536 continuous delayed images are sampled at the rate of f = 6.27 Hz ($fc/u_0 = 7.5$). The delayed images in either case are individually correlated with the average undelayed image of the stationary airfoil (512 images) at the AoA that is the same as α (for the stationary airfoil), and α_{eff} (for the moving airfoil). The camera exposure time for all measurements is in the range of 500 – 600 μs (held fixed between the undelayed and delayed images), and the delay time is in the range of 5 – 6 ms. The corresponding pixel displacement of the freestream flow is approximately 9 pixels (0.5% c). The sub-pixel displacement uncertainty in the mean based on a 95% confidence interval is estimated to be ±0.1 pixel for the plunging airfoil measurements, and ±0.04 pixel for the stationary airfoil measurements. These correspond to mean-streamwise-velocity uncertainties of less than ±0.14 cm/s, and ±0.06 cm/s, respectively. The uncertainty in the moving airfoil being at the same position in each image is limited only by the pixel resolution, since the encoder resolution, airfoil motion through image capture latency, and mechanical vibration combined are less than the sub-pixel displacement error. Between the undelayed and the delayed images, the moving airfoil translates 25 μm

(0.02% c), or 0.36 pixel. This motion is inherent to the experiment, and for the purposes of the correlation, the Lagrangian displacement remains computed in the direction normal to the undelayed tag line without adjusting the delayed lines.

The resulting streamwise velocity measurement for the plunging airfoil is in the laboratory frame of reference. To compare it to its stationary airfoil counterpart, the measurement is transformed to the GT frame by subtracting the airfoil velocity V_a, then rotated to obtain the streamwise velocity in the GT frame; i.e. the component aligned with the direction of u_{eff}. The latter is accomplished using axis-rotation transformation of the velocity vector components from the laboratory coordinate system (x, y) to the GT (x', y') coordinate system (see Fig. 3). Specifically, the streamwise velocity component for the moving airfoil in the GT frame should be calculated using:

$$u' = u\,cos(\alpha_i) + (v - V_a)\,sin(\alpha_i) \tag{2}$$

However, since v is not measurable using 1c-MTV, it is neglected in the transformation such that:

$$u' \cong u\,cos(\alpha_i) - V_a\,sin(\alpha_i) \tag{3}$$

Neglecting the contribution of v relative to u in calculating u' leads to an error of the order:

$$\frac{v\sin(\alpha_i)}{u\cos(\alpha_i)} = \left(\frac{v}{u}\right)\tan(\alpha_i) = \frac{v}{u}V_r \tag{4}$$

The freestream velocity component is generally the dominant component (except near the LE, and possibly near the separation and reattachment locations). Thus, the ratio v/u is expected to be small for most of the measurement domain. However, if this ratio is assumed to be unity to provide a conservative error estimate, the inaccuracy in the transformation is then of the order of the velocity ratio V_r, which is 5% in the present work.

IV. Results and Discussion

The results in Fig. 8 show a comparison of the mean-streamwise-velocity contours for the stationary and the moving airfoil at four different AoA. The contours are plotted using chord-wise and chord-normal (x^*, y^*) axes, and regions of reversed flow are given in purple to help identify the boundary layer separation zone. Overall, the flow is similar around the stationary and the plunging airfoil at the lower AoA (0° and 4°) (compare Fig. 8a and 8c, to 8b and 8d, respectively). We note that the difference marked in the separation location at zero AoA (approximately $0.23c$, given by red arrows) between the moving and stationary airfoil is not reliable for such thin separation regions, where insufficient spatial resolution, small uncertainty in the airfoil surface location and near-wall velocity measurement inaccuracy can lead to significant streamwise uncertainty in locating the separation point [17]. On the other hand, reattachment does not occur on the airfoil surface and the separation bubble is seen to remain open at α_{eff} = 0° and 4°, for both the stationary and the plunging airfoils. At $\alpha_{eff} = 4°$, differences between the stationary and the moving airfoil are difficult to distinguish beyond the uncertainty associated with the low sample size for the plunging airfoil case.

Figures 9a-d show the fluctuating-streamwise-velocity RMS contours at $\alpha_{eff} = 0°$ and 4°. At zero AoA, barely any flow unsteadiness is observed for both the stationary and the plunging airfoil. At $\alpha = 4°$, a pronounced increase in unsteadiness is seen, but the unsteadiness remains focused in a thin region above the airfoil surface corresponding to separated flow. Farther downstream, in the near wake, the unsteadiness spreads over a larger cross-stream domain. This is seen more clearly for the stationary airfoil (Fig. 9c), which has a measurement domain that extends farther downstream than the moving airfoil. Overall, the features of the u_{rms} results are similar for the stationary and the moving airfoil at $\alpha_{eff} = 0°$ and 4°. As discussed in connection with Fig. 1, the C_L on the plunging airfoil at low α_{eff} in shear is nearly identical to that of the stationary airfoil. In this low α_{eff} range, the similar lift coefficients on the stationary and the plunging airfoil are consistent with the similar characteristics of the mean and the RMS streamwise velocity fields.

Figures 8e-h show the mean velocity results at the larger AoA. The results between the stationary and the moving airfoil are strikingly different. For $\alpha_{eff} = 6°$, Fig. 8e shows a flow with open separation for the stationary airfoil. In stark contrast, Fig. 8f shows a flow characterized by separation and reattachment points closer to the LE for the plunging airfoil, creating a closed separation bubble on the airfoil. For $\alpha_{eff} = 8°$, in Fig 8g and 8h, both the stationary and the plunging airfoil show evidence of separation bubbles; however, the separation point on the plunging airfoil is

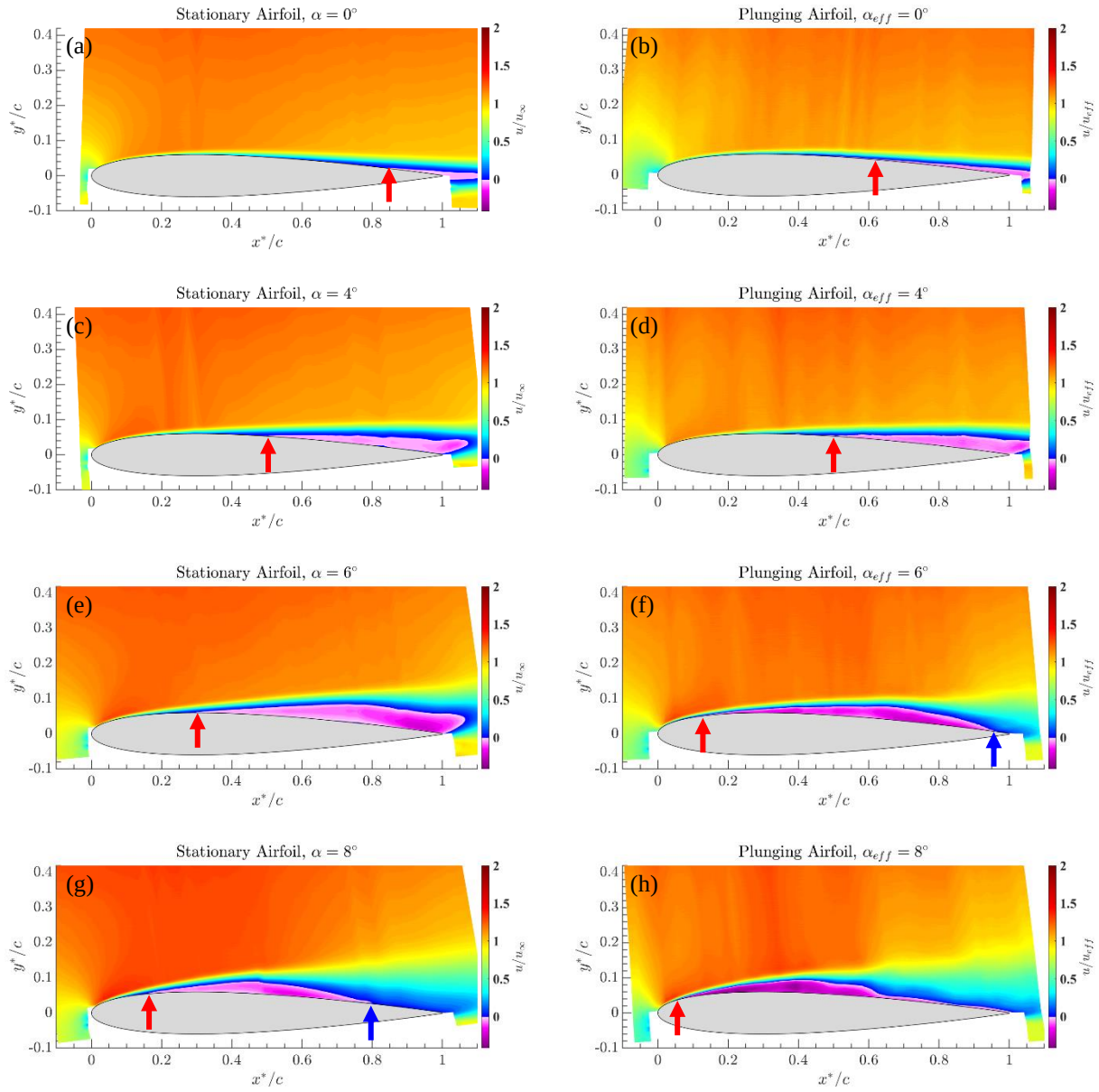

Fig. 8 Contour plots of the mean-streamwise-velocity around the stationary (left) and plunging (right) airfoils. Purple color indicates negative (reversed) flow to help identify the boundary layer separation zone. Red and blue arrows indicate approximate separation and reattachment points, respectively.

closer to the LE. The reattachment point of the plunging airfoil is unclear, as an unusual thin region of reversed flow is measured near the airfoil surface, extending from what would appear to be the end of the separation bubble, all the way to the TE. Inspection of the instantaneous streamwise velocity fields shows the flow to be highly unsteady in this region with alternating forward and reversed flow. Given this, it is suspected that more samples are needed for the measurements to converge in this case.

Differences between the stationary and the plunging airfoil at the higher AoA of 6° and 8° are also seen in the u_{rms} results in Figs. 9e-h. A general trend seen for both low and high AoA in Fig. 9 is that the location at which the thin zone of high RMS spreads relatively abruptly in the cross-stream direction moves upstream with increasing AoA, consistent with the upstream movement of the separation point. However, at 6° and 8°, this spread takes place farther upstream for the moving airfoil compared to the stationary airfoil, in accordance with the farther upstream location of the separation point on the moving airfoil compared to the stationary airfoil. This suggests that the airfoil movement causes the separating shear layer to transition earlier at the higher AoA. This conclusion is also supported by the occurrence of the maximum u_{rms} for the moving airfoil at a chord-wise location that is upstream of that of the

stationary airfoil. Another difference seen in the u_{rms} features is seen in the pre-transition thin region of high RMS, where this region is located closer to the airfoil surface for the plunging, in comparison to the stationary airfoil. The differences between the mean and the RMS streamwise velocity data for the stationary and the plunging airfoil at higher AoA are consistent with the corresponding difference in the C_L behavior in Fig. 1 at the same AoA.

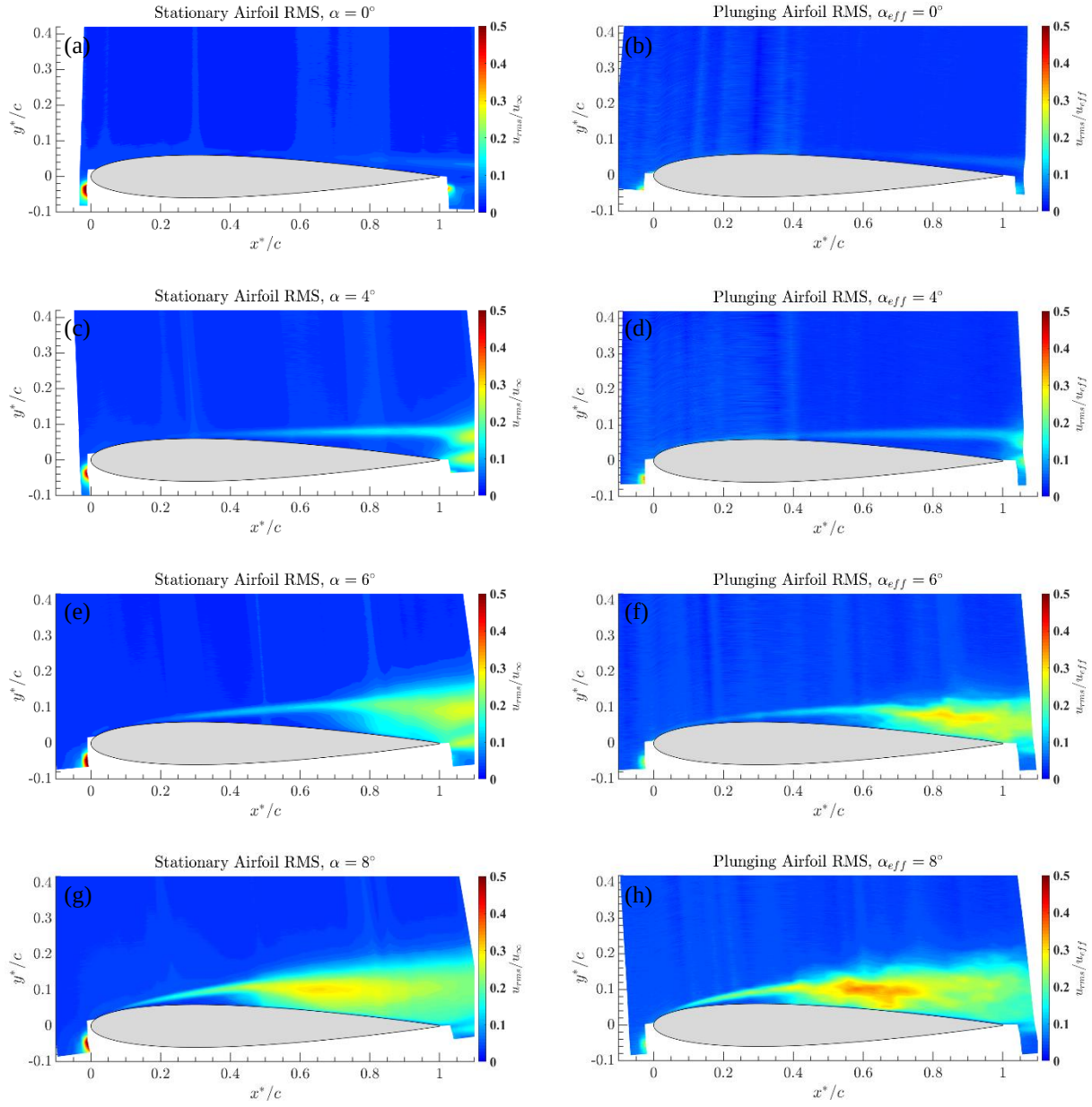

Fig. 9 Contour plots of the fluctuating-streamwise-velocity RMS around the stationary (left) and plunging (right) airfoils.

V. Conclusion

The results presented herein show that the fundamental fluid dynamics of the plunging airfoil in uniform-shear flow, in a Galilean reference frame, is different from that of the stationary airfoil at near-stall, positive effective angles of attack (α_{eff}). At small α_{eff}, the streamwise velocity of the flow over the stationary and the plunging airfoils are similar, consistent with their matching lift coefficients from Ref. [9]. As the airfoil approaches positive-α_{eff} stall, a

laminar separation bubble forms at a lower α_{eff} for the plunging airfoil compared to the stationary airfoil. This condition is also characterized by separation locations on the plunging airfoil closer to the LE compared to the stationary counterpart. The current flow measurements in this α_{eff} range support the lift coefficient measurements of Ref. [9], as the higher lift coefficient on the plunging airfoil corresponds to this separation bubble behavior. One limitation of the current study is the small sample size of the moving airfoil data, which constrains our ability to provide sufficiently converged mean- and fluctuating-velocity data when the flow is highly unsteady. This issue, which is encountered on the aft half of the airfoil at high α_{eff}, makes it difficult to unambiguously identify the reattachment location near, or at, stall conditions for the moving airfoil. Work is currently underway to devise methods to increase the sample size, which is limited by the long duration of the moving-airfoil experiments.

Acknowledgements

This work is supported by Office of Naval Research (ONR) grant number N00014-16-1-2760, and the NDSEG Fellowship Program with ONR as the sponsoring agency. The views and conclusions contained in this document are those of the authors and should not be interpreted as representing the official policies, either expressed or implied, of ONR or the U.S. Government. The U.S. Government is authorized to reproduce and distribute reprints for Government purposes notwithstanding any copyright notation herein.

References

[1] Frost, W., and Shabibi, A. M., "A Field Study of Wind Over a Simulated Block Building." NASA Report CR-2804, 1977 (https://ntrs.nasa.gov/search.jsp?R=19770011713)

[2] Woo H. G. C., Peterka, J. A., and Cermak, J. E., "Wind-Tunnel Measurements in the Wakes of Structures." NASA Report CR-2806, 1977 (https://ntrs.nasa.gov/search.jsp?R=19770012772)

[3] Garratt, J. R., "Review: the atmospheric boundary layer." *Earth Science Reviews*, Vol. 37, No. 1-2, pp. 89-134, 1994 (https://doi.org/10.1016/0012-8252(94)90026-4)

[4] Lehman, A. F., "An Experimental Study of the Dynamic and Steady-State Flow Disturbances Encountered by Aircraft during a Carrier Landing Approach." *Journal of Aircraft*, Vol. 3, No. 3, 1966 (https://doi.org/10.2514/3.43726)

[5] Cherry, B. E., and Constantino, M. M., "The Burble Effect: Superstructure and Flight Deck Effects on Carrier Air Wake." United States Naval Academy, Annapolis, MD, 2010

[6] Hammer, P. R., Visbal, M. R., Naguib, A. M., and Koochesfahani, M. M., "Lift on a Steady 2-D Symmetric Airfoil in a Viscous Uniform Shear Flow." *Journal of Fluid Mechanics*, Vol. 837, R2, 2018 (https://doi.org/10.1017/jfm.2017.895)

[7] Tsien, H.-S. "Symmetrical Joukowsky airfoils in shear flow." *Quarterly of Applied Mathematics*, Vol. 1, No. 2, 1943, 130–148

[8] Hammer, P. R., Olson, D. A., Visbal, M. R., Naguib, A. M., and Koochesfahani, M. M. "Joint Computational-Experimental Investigation of Harmonically Pitching Airfoil Aerodynamics in Uniform-Shear Approach Flow." *AIAA Journal*, Vol. 57, No. 8, 2019, pp. 3290-3298 (https://doi.org/10.2514/1.J058232)

[9] Albrecht M. B., Naguib, A. M., and Koochesfahani, M. M., "A Study of the Aerodynamics of a Low Reynolds Number Airfoil Translating Across a Uniform-Shear Approach Flow." 2019 AIAA Aerospace Sciences Meeting, AIAA SciTech Forum, (AIAA 2019-2157) (https://doi.org/10.2514/6.2019-2157)

[10] Hamedani, B. A., Naguib, A. M., and Koochesfahani, M. M., "Reynolds Number Effect on Lift Characteristics of an Airfoil Translating Across a Non-uniform Approach Flow." 2019 AIAA Aerospace Sciences Meeting, AIAA SciTech Forum, (AIAA 2019-0639) (https://doi.org/10.2514/6.2019-0639)

[11] Naguib, A. N., Koochesfahani, M. M., "Inviscid flow analysis of a circular cylinder traversing across an unbounded uniform-shear stream." *Journal of Fluid Mechanics*, Vol. 882, A21, 2020 (https://doi.org/10.1017/jfm.2019.820)

[12] Kotansky, D. R. "The use of honeycomb for shear flow generation." *AIAA Journal*, Vol. 4, No. 8, 1966, pp. 1490-1491. (https://doi.org/10.2514/3.3724)

[13] Safaripour, A., Olson, D., Naguib, A., and Koochesfahani, M. "On Using Shaped Honeycombs for Experimental Generation of Arbitrary Velocity Profiles in Test Facilities." *Bulletin of American Physical Society*. Vol. 61, No. 20, 2016, p. 265. (http://meetings.aps.org/link/BAPS.2016.DFD.G31.6)

[14] Gendrich, C. P., Koochesfahani, M. M., and Nocera, D. G. "Molecular tagging velocimetry and other novel applications of a new phosphorescent supramolecule." *Experiments in Fluids*, 23:675–691, 1997. (https://doi.org/10.1007/s003480050123)

[15] Koochesfahani, M. M., and Nocera, D. G. "Molecular tagging velocimetry." In: Tropea, C., Yarin, A. L., Foss, J. F. (eds) *Handbook of Experimental Fluid Dynamics*, Chap 5. Springer, Berlin Heidelberg, 2007, pp 362–382. (https://doi.org/10.1007/978-3-540-30299-5)

[16] Gendrich, C. P., and Koochesfahani, M. M. "A spatial correlation technique for estimating velocity fields using molecular tagging velocimetry (MTV)." *Experiments in Fluids*, 22(1), 1996, 67-77. (https://doi.org/10.1007/BF01893307)

[17] Olson, D.A., Katz, A.W., Naguib, A.M. et al. "On the challenges in experimental characterization of flow separation over airfoils at low Reynolds number." *Experiments in Fluids*, 54: 1470, 2013. (https://doi.org/10.1007/s00348-013-1470-1)